First-principles Studies on Molecular Beam Epitaxy Growth of $GaAs_{1-x}Bi_x$

Guangfu Luo,[1] Shujiang Yang,[1] Jincheng Li,[2] Mehrdad Arjmand,[3] Izabela Szlufarska,[1] April Brown,[2] Thomas F. Kuech,[4] Dane Morgan[1,*]

[1]*Department of Materials Science and Engineering, University of Wisconsin-Madison, Madison, Wisconsin 53706, USA*

[2]*Department of Electrical and Computer Engineering, Duke University, Durham, North Carolina 27709, USA*

[3]*Department of Engineering Physics, University of Wisconsin-Madison, Madison, Wisconsin 53706, USA*

[4]*Department of Chemical and Biological Engineering, University of Wisconsin-Madison, Madison, Wisconsin 53706, USA*

*Corresponding author. Tel.: +1-608-265-5879. E-mail address: ddmorgan@wisc.edu

Abstract

We investigate the molecular beam epitaxy (MBE) growth of $GaAs_{1-x}Bi_x$ film using density functional theory with spin-orbit coupling to understand the growth of this film, especially the mechanisms of Bi incorporation. We study the stable adsorption structures and kinetics of the incident MBE species (As_2 molecule, Ga atom, Bi atom, and Bi_2 molecule) on the (2×1)-Ga_{sub}||Bi surface and a proposed q(1×1)-Ga_{sub}||AsAs surface, where $Ga_{sub}||XY$ refers to a Ga-terminated GaAs(001) substrate with surface layers of X and Y. The q(1×1)-Ga_{sub}||AsAs surface has a quasi-(1×1) As layer above the Ga-terminated GaAs substrate and a randomly-oriented As dimer layer on top. We obtain the desorption and diffusion barriers of the adsorbed MBE species and also the reaction barriers of three key processes related to Bi evolution, namely, Bi incorporation, As/Bi exchange, and Bi clustering. The results help explain the experimentally observed dependence of Bi incorporation on the As/Ga ratio and growth temperature. Furthermore, we find that As_2 exchange with Bi of the (2×1)-Ga_{sub}||Bi surface is a key step controlling the kinetics of the Bi incorporation. Finally, we explore two possible methods to enhance the Bi incorporation, namely, replacing the MBE growth mode from co-deposition of all fluxes with a sequential deposition of fluxes and applying asymmetric in-plane strain to the substrate.

PACS numbers: 68.43.Bc, 81.15.Aa, 81.15.Hi

I. INTRODUCTION

Bi-doped GaAs, $GaAs_{1-x}Bi_x$, has been widely explored in recent years for applications in semiconductor devices due to a number of exceptional properties of this compound. First, Bi atoms incorporated into GaAs lead to a significantly reduced (~84 meV per Bi%) [1-5] and temperature-insensitive [4-10] band gap. Furthermore, because of the very large spin-orbit (SO) splitting of Bi atoms, the serious efficiency decrease, known as efficiency droop, in telecommunication lasers caused by Auger recombination can potentially be suppressed for $GaAs_{1-x}Bi_x$ with $x > 11\%$ [11]. Finally, the Bi incorporation also remarkably decreases the spin relaxation time and thus leads to a longer lifetime of spin states by modification of SO interaction [12]. These features make $GaAs_{1-x}Bi_x$ a promising material for solar cells, laser diodes, infrared light-emitting diodes, and spintronic devices.

However, incorporating a high fraction of Bi (close to 10%) and maintaining good structural, electronic, and optical quality have been a longstanding challenge. Previous *ab initio* calculations predicted that the equilibrium solubility of Bi atom in GaAs is less than 0.01% under Ga- and Bi-rich conditions at 400 ºC [13], primarily due to a 24.4% larger covalent radius of Bi than As [14]. A much greater amount of Bi have been incorporated in growth far from equilibrium, such as metalorganic vapor-phase epitaxy [3, 5-8, 10, 15-18] and molecular beam epitaxy (MBE) [4, 9, 19-27]. Recently, optically active $GaAs_{1-x}Bi_x$ films with 11% Bi have been fabricated [24-26] and optically inactive films with 22% Bi have also been reported [27]. Nevertheless, in these high Bi-content films, Bi and/or Ga droplets are frequently formed on film surface [25, 27, 28], the carrier lifetime is usually very short, and abundant non-radiative recombination centers that lead to low photoluminescence intensity exist [24, 29]. Partial cause of these structural, electronic, and optical issues is that present conditions allowing incorporation of a high Bi content are low temperature and near unity As/Ga ratio [19, 25], which are not ideal conditions to grow GaAs.

Because of the above-mentioned growth challenges, understanding the kinetics of Bi incorporation under nonequilibrium conditions is highly desirable to guide the growth of high-quality films with increased Bi content. Lu *at al*. [25] and Lewis *et al*. [27] have proposed empirical models for $GaAs_{1-x}Bi_x$ growth and used them to explain the saturation of Bi incorporation and explore conditions to increase the Bi content. However, majority of the assumptions and parameters in these models are still unverified and the atomistic calculations performed here suggest that several fundamental assumptions of the models need to be reconsidered (a detailed discussion is given later in this article). To better understand the nonequilibrium MBE growth of $GaAs_{1-x}Bi_x$, we use first-principles calculations to (1) examine surface reconstructions during growth, (2) identify the stable adsorption sites and desorption barriers of the MBE species, (3) obtain surface diffusion of the MBE species, and (4) explore the essential kinetic processes

related to Bi evolution during growth. We finally analyze the implications of our results and propose methods to enhance the Bi incorporation and meantime reduce defects in the films.

II. COMPUTATIONAL DETAILS

In order to maximize the relevance of our modeling, we refer to the conditions used in recent MBE experiments performed by some of the authors [30], which are similar to those widely used in the growth of $GaAs_{1-x}Bi_x$ [19, 25, 26, 31]. In the experiments [30], the GaAs(001) substrate maintains a temperature of 320 °C. The As, Ga, and Bi beams are in the form of As_2 molecules, Ga atoms, and Bi atoms and Bi_2 molecules approximately in the same amount, respectively. The flux ratio of Ga beam is about 1 ML/s and the flux ratio of As:Ga:Bi is estimated to be 1:1:1/20. The As, Bi, and Ga beams are opened sequentially and all beams remain open in the co-deposition growth mode. Before the opening of Ga beam, about a 38% monolayer of Bi on the As or Ga sites is deposited. During the growth, the reflection high-energy electron diffraction (RHEED) keeps a (2×1) pattern, which is consistent with previous experiments below 400 °C and at nearly unity As/Ga flux ratio [31, 32]. Given such experimental conditions, our theoretical modeling will focus on surfaces under conditions of 320 °C and flux ratio As:Ga ≈ 1:1.

Our first-principles calculations are carried out using density functional theory (DFT) with the Vienna Ab-initio Simulation Package [33]. The calculations are performed using the local density approximation and the projector augmented wave potential [34] with configurations of Ga($4s^2 4p^1$), As($4s^2 4p^3$), and Bi($4s^2 4p^3$). The plane-wave energy cutoff is set to 400 eV. Spin-orbit coupling is included to describe the strong relativistic effects in Bi atoms, which influence the energetics quite significantly. Specifically, changes associated with SO coupling are up to 1.07 eV in the binding energy and up to 0.31 eV in the activation barrier [35]. The Ga-terminated GaAs(001) substrate is simulated with five III-V atomic layers, with the bottom layer passivated with pseudo-hydrogen atoms [36, 37]. The in-plane cell size is fixed to a 4 × 4 unit cell of the bulk (15.914 Å × 15.914 Å and 128 atoms in total) and is increased to a 4×6 unit cell of the bulk (15.914 Å × 23.872 Å and 192 atoms in total) for Bi trimer simulations. The atomic positions are fixed for the pseudo-hydrogen atoms and two bottom Ga/As layers, while other atoms are relaxed till the force on each atom is less than 0.005 eV/Å. A vacuum layer as thick as 10 Å is added above the surface. The *k*-point sampling is a gamma-centered 3 × 3 × 1 grid for the 128-atom slab and 3×2×1 grid for the 192-atom slab. The binding energy E_b of a MBE species on a surface is defined by the following equation,

$$E_b = E_{\text{surface+molecule}} - E_{\text{surface}} - E_{\text{isolated-molecule}}, \quad (1)$$

where E_X is the internal energy of system X at a temperature of 0 K. The desorption barrier at 0 K is obtained from the minimum energy path as an ad-species is pulled away from a surface, and the limited temperature effect on the desorption barrier will be discussed later in this article. Transition state theory

with an attempt frequency of 10^{12} Hz at the temperature 320 °C is used to estimate the time scales of elementary processes. The climbing nudged elastic band method [38] is used to calculate activation barriers.

III. RESULTS AND DISCUSSIONS

A. Structure of the Surface

At the beginning of our modelling, it is important to establish the surfaces present during growth on the GaAs(001) substrate. A number of authors have suggested that significant Bi atoms exist on the $GaAs_{1-x}Bi_x$ surface during growth [25, 27, 39]. In support of this statement, we summarize the strong evidence as follows. First, Bi atoms have a well-established surfactant effect in the growth of GaAs, where Bi atoms float on the top and enhance the smoothness of the GaAs surface [40]. This result indicates that at least some Bi atoms tend to reside on the surface of a growing $GaAs_{1-x}Bi_x$ film. Second, given the initial Bi deposition (38% monolayer coverage), Bi flux (1/20 of the Ga flux), Bi incorporation ratio (~3%) [30], and the negligible desorption ratio (see later discussion), unincorporated Bi must be building up on the surface. Third, previous experiments observed that at low T (< 400 K) and As-deficient conditions, a Bi-terminated surface on GaAs(001) possesses a (2×1) reconstruction, which does not appear in the growth of GaAs [31, 41, 42]. Because a (2×1) reconstruction was also observed under the same growth conditions modelled here, it is reasonable to attribute the (2×1) pattern to Bi-terminated areas.

However, controversial statements still exist in literature about the layer composition below the (2×1) Bi surface. Previous models [25, 27] assumed that the layers starting from the top are Bi, As, and Ga. We denote this ordering as $Ga_{sub}||AsBi$ (Fig. 1a), where $Ga_{sub}||XY$ refers to a Ga-terminated GaAs(001) substrate with surface layer of X and Y. The assumption of a $Ga_{sub}||AsBi$ stacking is reasonable at the very early stages of growth due to the first opening of the As beam and the following opening of the Bi beam. However, recent theoretical study of Bi-terminated GaAs(001) found that $Ga_{sub}||Bi$ (Fig. 1b) is the only stable (2×1) Bi surface [43]. Our calculations further indicate that a Ga adatom can easily exchange with a Bi atom of the $Ga_{sub}||AsBi$ with a significant driving force (0.37–0.71 eV) and very low activation barriers (0.08–0.11 eV) [35]. Therefore, after deposition of a complete additional Ga layer on the $Ga_{sub}||AsBi$, the surface is expected to transform to $Ga_{sub}||AsGaBi$, a structure equivalent to $Ga_{sub}||Bi$. Based on these calculation results, it is likely that the Bi-terminated surface during growth is the (2×1)-$Ga_{sub}||Bi$ surface.

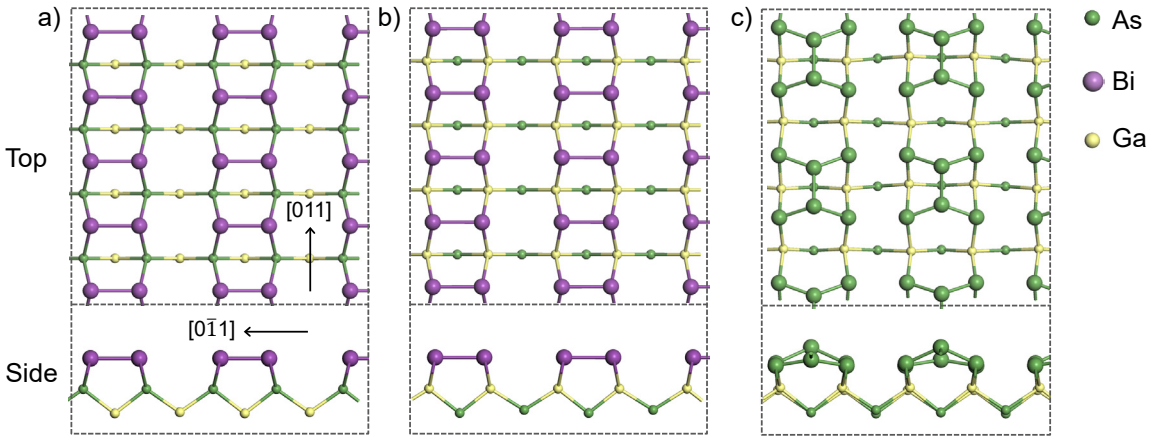

FIG. 1. (Color online) Structures of the (a) (2×1)-Ga_{sub}||AsBi, (b) (2×1)-Ga_{sub}||Bi, and (c) short-range ordered q(1×1)-Ga_{sub}||AsAs surfaces. Several bottom layers are hidden for easy visualization.

Since the deposited Bi atoms are insufficient to form a complete Bi layer on the epitaxial film at the start of growth and may remain so during growth, it is important to consider areas that are not Bi-terminated. The exact nature of the non-Bi terminated surface is unclear, but due to the ubiquitous presence of As_2 molecules in the system, we assume a portion of the surface to be As-terminated. Previous experiments suggest that an As-terminated region has a (1×1) reconstruction under the conditions of $T < 400$ K and near unity As/Ga ratio [31, 44].

Relative to the (2×1)-Ga_{sub}||Bi surface, the structure of (1×1) As surface has been much less explored in the literature and an atomically resolved structure is still unknown [31, 44]. However, the limited literature combined with our computational studies provides some constraints to the candidate structure. First, previous low-energy electron diffraction (LEED) experiments [45] found that in additional to a (1×1) pattern, faint half-integer spots and background were also observed. Second, our calculations show that a bulk-like (1×1) As surface on a Ga-terminated substrate is unrealistic and small perturbations in atomic positions lead to formation of As dimers, which break the (1×1) symmetry. Finally, a previous study by Morgan, *et al.* proposed that the change of As-terminated c(4×4) surface to a (1×1) surface during the cooling of the GaAs surface in As_2 gas occurred by random As_2 adsorption [46].

Given the above constraints, we propose to model the (1×1) As surface as a two As-layer structure following the idea suggested by Morgan, *et al.* [46]. Specifically, the top layer consists of As_2 with a local (2×2) reconstruction (Fig. 1c) to yield the faint half-integer spots but also consists of small domains of this structure not to generate any additional strong pattern. The second from the top layer possesses a quasi-(1×1) structure, which, as opposed to a perfect (1×1) order, is attributed to the small distortions from the top layer. We denote this surface as q(1×1)-Ga_{sub}||AsAs. To demonstrate that this model can reproduce the observed LEED pattern [45], we construct a large surface consisting of domains of the structure shown in Fig. 1c with random orientations along [011] and [0$\bar{1}$1], as shown in Fig. 2a. Figure 2b

shows its simulated LEED image, where the strong (1×1) pattern and faint half-integer spots are observed. This model is consistent with Morgan *et al*'s qualitative model [46] and addresses the two critical constraints discussed above for the (1×1) As-terminated surface: (1) Both the top and the second from the top layers are stabilized; (2) The second from the top layer generates a strong (1×1) LEED pattern and the top layer generates weak half-integer spots and background. Experimentally, the weak half-integer spots and background could be missed and only the strong (1×1) pattern is observed, as found in the previous study [45]. Due to the difficulty of simulating a large disordered structure using *ab initio* method, we will perform DFT calculations using the ordered structure shown in Fig. 1c.

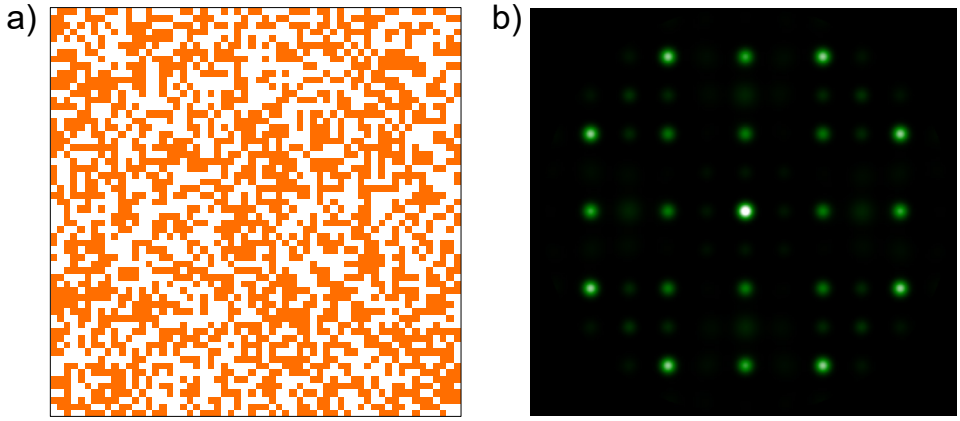

FIG. 2. (Color online) Verification of the proposed As surface model. (a) Randomly oriented As_2 layer of the $q(1\times1)$-Ga_{sub}||AsAs surface. The orange and white areas have perpendicular orientations. Each side has a length of ~955Å. Atomic positions of each unit domain are from the relaxed structure of Fig. 1c. (b) Simulated LEED pattern corresponding to the surface in panel (a) using the code RHEEDsim [47]. In the simulation, a radius of 6 for the LEED film, a pixel density of 600×600 for the plot, a broadening parameter of 0.1, and a mesh grid of 1200×1200 for reciprocal vectors are used.

Based on the aforementioned discussions, we assume that the general surface consists of the (2×1)-Ga_{sub}||Bi and $q(1\times1)$-Ga_{sub}||AsAs regions. Because the major (1×1) pattern from the As region is a subset of the (2×1) pattern from the Bi region, their coexistence shows a superimposed (1×1) and (2×1) RHEED or LEED pattern. This pattern could easily appear as pure (2×1), especially for if there are more (2×1)-Ga_{sub}||Bi than $q(1\times1)$-Ga_{sub}||AsAs regions. Band structures in Fig. 3 show that the (2×1)-Ga_{sub}||Bi surface is metallic and the $q(1\times1)$-Ga_{sub}||AsAs and (2×1)-Ga_{sub}||AsBi surfaces are semiconducting. These electronic structure predictions can potentially be verified by scanning tunneling microscopy, making the proposed surface structures testable by experiments.

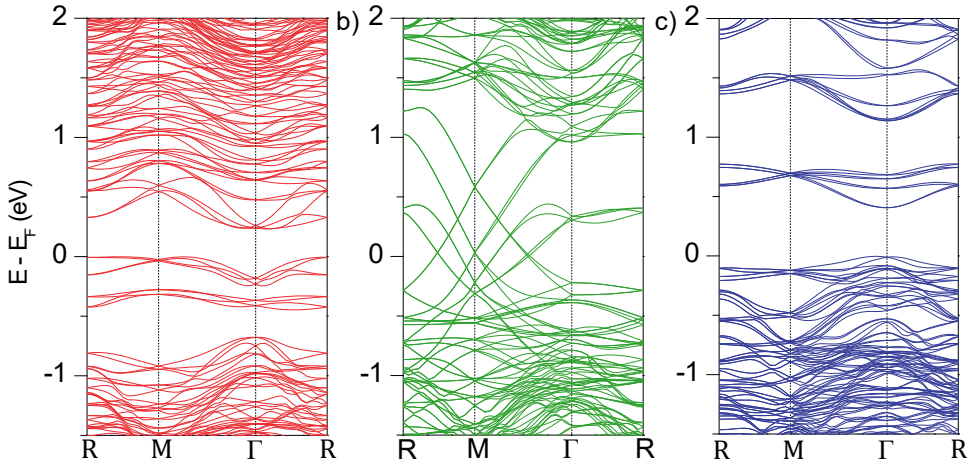

FIG. 3. (Color online) Band structures of the (a) (2×1)-Ga_{sub}||AsBi, (b) (2×1)-Ga_{sub}||Bi, and (c) *q*(1×1)-Ga_{sub}||AsAs surfaces. E_F represents the Fermi energy. *R*=(1/2, 0, 0), *M*=(1/2, 1/2, 0), and *Γ*=(0, 0, 0).

B. Adsorption and Desorption

To understand the growth behavior, it is necessary to explore where the species adsorb and how strongly they bind to the surface. Figure 4 shows the stable adsorption sites and binding energies of Bi, Ga, As_2, and Bi_2 on the (2×1)-Ga_{sub}||Bi and *q*(1×1)-Ga_{sub}||AsAs surfaces at 0 K. We systematically search the adsorption sites by sampling the whole surface and care is taken to slightly break the symmetry of initial structures to enable the finding of stable local minima. We find that the most stable adsorption sites are in the trench, a space between two dimer rows, except As_2 on the Bi surface, which has almost the same binding energy in the trench as on the dimer row.

Generally, all species adsorb strongly on the two surfaces with binding energy ranging from -4.79 to -1.71 eV. Calculations indicate that at 0 K, the desorption barrier of each species equals the absolute value of its binding energy [35]. The temperature effects are difficult to calculate quantitatively, but based on detailed studies for desorption of CO from the Ru(0001) surface [48], we estimate the effect on desorption barrier to be about 0.3 eV at 320 ºC. The large desorption barriers at 0 K combined with the limited temperature impact suggest that these chemically adsorbed species seldom leave the surface during growth. This result does not contradict the evaporation of As_2 found in experiments, because As_2 can also physisorb on the surface, from which state it can easily desorb [46].

We find that all species adsorb much stronger (0.72~2.76 eV) on the As surface than on the Bi surface. For comparison, we also indicate the second most stable adsorption sites. It is readily seen that the adsorption of the second most stable sites are also much stronger (0.45~2.15 eV) on the As surface than on the Bi surface. Since surface diffusion generally correlates with surface binding [49], these results suggest that diffusion will be possibly faster on the Bi surface than on the As surface, as confirmed in the following section.

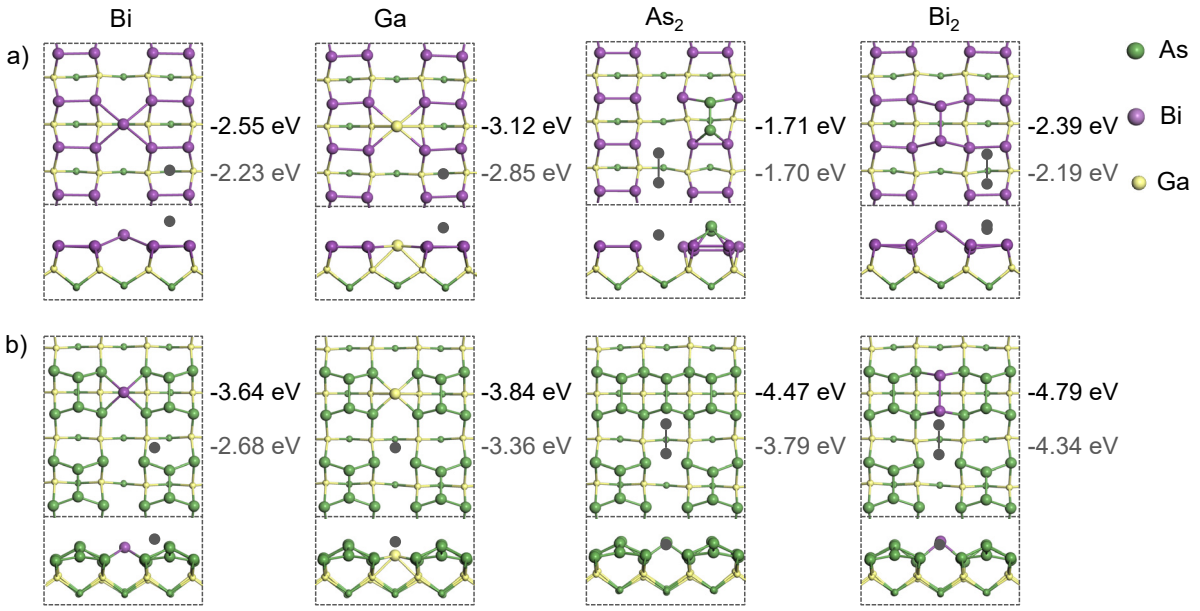

FIG. 4. (Color online) The most and second most stable adsorption sites and associated binding energies per Bi, Ga, As_2 and Bi_2 on the (a) (2×1)-Ga_{sub}||Bi and (b) (1×1)-Ga_{sub}||AsAs surfaces. The second most stable positions and binding energies are shown in gray.

C. Surface Diffusion

To understand the growth kinetics we now consider the surface diffusion. As listed in Table I, the MBE species have relatively small diffusion barriers of 0.19−0.73 eV (corresponding to about 4.1×10^{-11}−1.6×10^{-6} s per jump) on both surfaces, except Bi_2 and As_2 on the As surface, which possess barriers of 1.63 and 2.70 eV (corresponding to 71 and 8.9×10^{10} s per jump), respectively. Given the fast diffusivities, we expect that the Bi and Ga adatoms can transfer quickly between the Bi and As surfaces and the distribution on the two surfaces can be calculated from thermodynamics according to their binding energies. Due to their high diffusion barriers, the As_2 and Bi_2 molecules are expected to stick near their deposited sites on the As surface and there is no transfer between the As and Bi surfaces. The animations of selected dynamic processes listed in Table I are illustrated in the Supplemental Material [35].

TABLE I. Binding energies and activation barriers of different processes on the (2×1)-Ga_{sub}||Bi and q(1×1)-Ga_{sub}||AsAs surfaces for the MBE species. Trench 1 and 2 of the As surface correspond to the trench along [011] and [$0\bar{1}1$], respectively. All energies are in units of eV. Desorption energies are equal to the corresponding absolute values of binding energy and are therefore not listed explicitly.

Species	Process	On Bi surface		On As surface	
		Trench	Dimer row	Trench 1	Trench 2

Bi	Bind	-2.55	-2.23	-3.64	-2.68
	Diffuse	0.53	0.19	0.68	–
	Dimerize	0.31-0.43	0.02-0.53	–	–
Ga	Bind	-3.12	-2.85	-3.84	-3.17
	Diffuse	0.27	0.40	0.65	0.40
	Incorporate	0	0	–	–
As_2	Bind	-1.70	-1.71	-4.47	-2.12
	Diffuse	0.36	0.73	2.70	–
	Exchange	0.65	0.58	–	–
Bi_2	Bind	-2.39	-2.19	-4.79	-2.47
	Diffuse	0.55	0.67	1.63	–

D. Incorporation, Exchange, and Clustering of Bi

Now we consider three general processes related to Bi evolution on the (2×1)-Ga_{sub}||Bi surface: the incorporation, exchange, and clustering of Bi, which are defined as Bi atom stabilization by Ga ad-atoms, Bi atom swapping from an underneath layer to the surface, and development of Bi clusters, respectively.

To model Bi incorporation, we consider a Ga adatom on the (2×1)-Ga_{sub}||Bi surface. We find that Ga atom forms four Ga-Bi bonds with the Bi surface without any energy barrier for the two most stable adsorption sites shown in Fig. 4a. Therefore, as soon as a Ga atom arrives on the Bi surface, the Bi is effectively incorporated into GaAs structure by the covering Ga adatom. This result suggests that most Bi atoms on the surface could be incorporated if the competing Bi exchange mechanism were efficiently avoided.

For the Bi exchange processes, among the four MBE species (Bi, Bi_2, As_2, and Ga), only As_2 and Ga could induce the Bi exchange, because the exchanges induced by Bi and Bi_2 cause no structural difference and thus are not important here. We first consider the exchange of an As_2 with the (2×1)-Ga_{sub}||Bi surface. For As_2 on the dimer row (Fig. 5a), one As atom (labeled as 2) first moves downward, then the As_2 rotates about 80° and moves downward further to squeeze out a Bi atom (labeled as 3). Meanwhile, the Bi atom forms an As-Bi bond with another As atom (labeled as 1) of the As_2. Finally, the As-Bi bond rotates about 43° and stabilizes on the dimer row with a structure similar to the initial state. This exchange pathway has a 0.56 eV lower final state than the initial one and a 0.58 eV rate-determining barrier, which suggest a favorable and very fast reaction occurring at the time scale of ~8.5×10^{-8} s.

For As_2 in the trench (Fig. 5b), the As_2 first moves downward and tilts slightly, then one As atom (labeled as 1) closer to a dimer row moves downward to squeeze out a Bi (labeled as 3). Subsequently, the other As atom (labeled as 2) moves upward toward the squeezed-out Bi and forms a new As-Bi bond. Finally, the new As-Bi bond rotates about 70° and reaches a final state same as the final one in Fig. 5a. This pathway has a 0.58 eV lower final state than the initial one and a 0.65 eV rate-determining barrier, which again suggest a favorable and fast process occurring at the time scale of ~3.3×10^{-7} s.

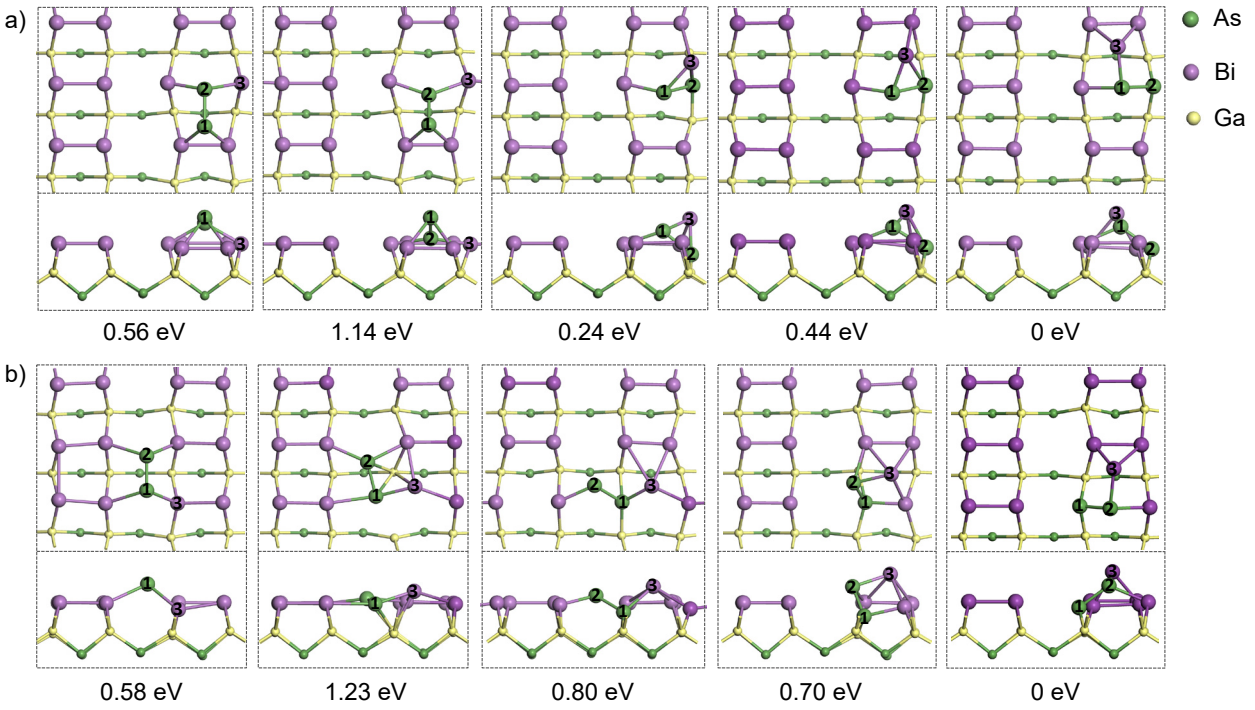

FIG. 5. (Color online) As_2 exchange with a Bi of the (2×1)-Ga_{sub}||Bi surface with the As_2 (a) on the dimer row and (b) in the trench. Energies of all structures relative to the lowest one are indicated below each panel, so do the figures about dynamic process in the rest of this article. Several atoms are numbered to guide the eyes.

The aforementioned two pathways are for the initial stage of As_2-induced exchange on a perfect Bi surface. To assess the opposite extreme, e.g. a previous Bi-terminated region being close to be completely exchanged, we examine a surface with one Bi atom surrounded by As atoms, i.e. a (2×1)-Ga_{sub}||As region with one Bi substituted for As. Under such conditions, a similar process to the one in Fig. 5a has a higher barrier of 0.96 eV [35] than the barrier of 0.58 eV in Fig. 5a, but this process still occurs quickly (~1.4×10^{-4} s per exchange) relative to the growth rate of ~1 ML/s. Assuming that more complex surface structures with mixed As and Bi in the surface layer (i.e. Ga_{sub}||(As,Bi) surfaces) yield barriers between the two extremes, we anticipate that the As_2-induced Bi exchange processes are very rapid.

Ga adatom exchange with the underlying Bi atom is expected to be unfavorable as it leads to a Ga antisite. Consistent with this expectation, calculations show that such exchange reaction possesses a 0.64 eV barrier and a finial state 0.32 eV higher in energy than the initial state [35]. These values suggest that although such exchanges can occur, the Ga will rarely stay on the Bi site due to the increased energy and will tend to rapidly swap back with the Bi. As a result, our calculations predict that As_2 is the only dominant MBE species inducing fast Bi exchange processes.

Bi clustering is the beginning stage of Bi droplet formation and may generally occur during the growth. Here, we investigate the formation of Bi dimers and trimers. We first try to answer which types of Bi source on the surface, the (2×1)-Ga_{sub}||Bi surface or Bi adatoms, might more rapidly form the dimers and trimers. To explore if the Bi surface is unstable and can spontaneously transform to Bi clusters, we consider a process shown in Fig. 6a: a Bi atom hopping to a local minimum nearby and leaving a vacancy behind, which is a critical process assumed in the empirical growth model by Lewis *et al*. [27]. Our calculations indicate that this pathway has a 1.30 eV barrier and a final state higher by 1.24 eV than the initial state, suggesting that this process will not occur for a significant number of Bi atoms. We also consider another pathway with a Bi jumping above the dimer row, but it is so unstable that the final state returns to the initial one without finding a local minimum [35]. These results suggest that the Bi surface is stable and will not evolve to form Bi clusters spontaneously.

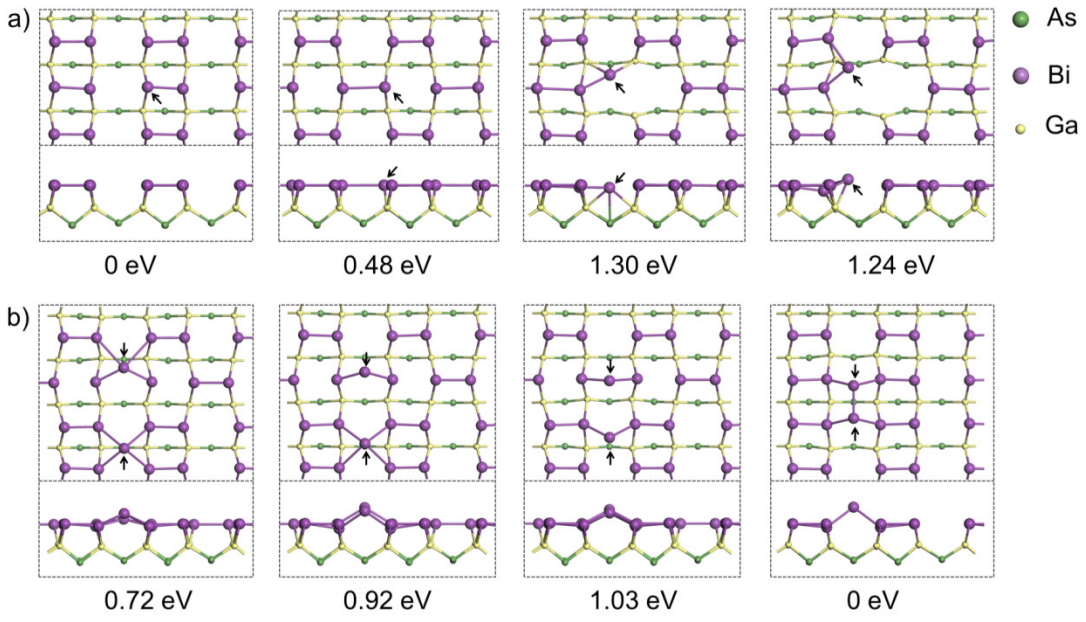

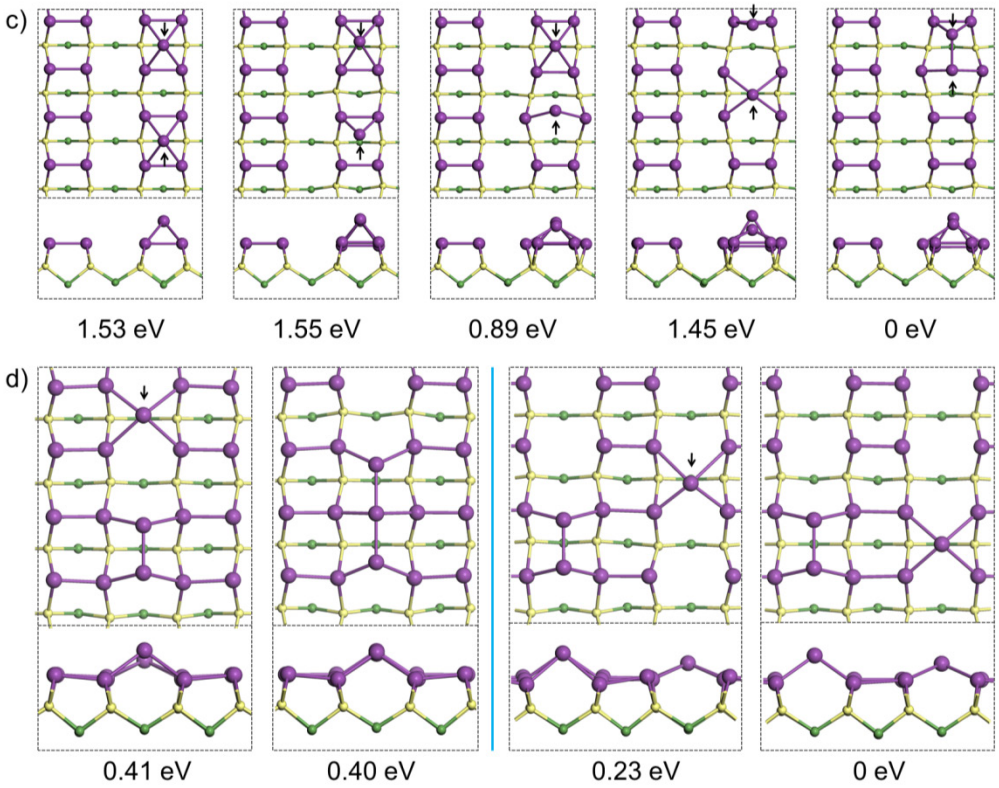

FIG. 6. (Color online) (a) One Bi atom jumping out of the (2×1)-Ga_{sub}||Bi surface. (b) Dimerization of two Bi adatoms in the trench of the (2×1)-Ga_{sub}||Bi surface. If the two Bi adatoms are completely isolated in the initial state, the corresponding energy is 0.60 eV. (c) Dimerization of two Bi on the dimer row of the (2×1)-Ga_{sub}||Bi surface. If the two Bi adatoms are completely isolated in the initial state, the corresponding energy is 1.02 eV. (d) Attachment of a third Bi adatom to a Bi dimer from the same or from a neighboring trench. Only initial and final states are shown here.

Next we consider the assembly of adsorbed Bi/Bi_2 on the Bi surface. Figure 6b shows the dimerization of two Bi adatoms in the trench of the Bi surface, which has a final state 0.72 eV lower than the initial one and an activation barrier of 0.31 eV. If the two Bi adatoms are initially separated far enough so that their mutual interaction is negligible, the energy decrease of the final state is 0.60 eV and overall barrier is 0.43 eV. When the dimerization occurs between nearby Bi adatoms on the dimer row, the process has a final state 1.53 eV lower the initial one and an overall barrier of 0.02 eV (Fig. 6c). If the two Bi adatoms are initially separated far away, the energy decrease of the final state and overall barrier change to 1.02 eV and 0.53 eV, respectively. These results demonstrate that dimerization of Bi adatoms on the Bi surface has a strong driving force and occurs very fast.

Figure 6d shows a Bi adatom joining to an existing Bi_2 either from the same or from a neighboring trench of the Bi_2. Both pathways have the same reaction barriers of 0.30 eV. However, the energy

decrease is only 0.01 eV for Bi from the same trench but 0.23 eV for Bi from a neighboring trench. This result suggests that Bi clustering initially occur perpendicular to the Bi dimer row due to the increased stability along this direction.

E. Possible Growth Processes

Based on the aforementioned energetic and kinetic results, we anticipate several processes during the growth. Because Ga and Bi adatoms diffuse fast (< 6.0×10^{-7} s per hop) on both the Bi and As surfaces, they will quickly reach equilibrium on the two surfaces, with occupations following Boltzmann statistics. Due to the significantly stronger binding on the As surface, Ga and Bi adatoms may concentrate mainly on the As surface in the initial growth of a Ga layer, as schematically shown in Fig. 7a. As_2 and Bi_2 diffuse extremely slowly (> 71 s per hop) on the As surface and they will likely stay where they are deposited. As_2 should exchange quickly with the Bi surface in the initial growth of a Ga layer due to the low reaction barriers. When an increasing number of Ga atoms are deposited on the Bi surface, As_2 may react with Ga adatoms and consequently stop the exchange process (Fig. 7b). For Bi and Bi_2 on the Bi surface, their fast diffusion and low barriers of dimerization/trimerization can quickly lead to formation of Bi clusters (Fig. 7c).

Two important implications can be derived from the processes identified above. First, if the As flux is increased, the exchange process will occur faster and consequently lead to a lower incorporation of Bi, in agreement with previous experiments [25, 27, 50]. Second, because As_2 in the trench of Bi surface has a diffusion barrier of 0.36 eV and an exchange barrier of 0.65 eV, the times of hopping before each exchange process can be approximated by $t_{exch} / t_{hop} = e^{0.65\text{eV}/k_BT} / e^{0.36\text{eV}/k_BT} = e^{0.29\text{eV}/k_BT}$, where t_{exch} and t_{hop} are the time of each exchange and hopping, respectively. Therefore, on the (2×1)-Ga_{sub}||Bi surface, t_{exch}/t_{hop} and the associated diffusion length of As_2 before a Bi exchange process are greater at lower temperature. For example, t_{exch}/t_{hop} is ~292 at 320 °C but is greatly increased to ~1230 at 200 °C. For As_2 on the dimer row, because the diffusion barrier (0.73 eV) is greater than the exchange barrier (0.58 eV), its diffusion length is very short over a wide temperature range. An overall consequence of the above-mentioned kinetics is that at a lower temperature, As_2 has a longer diffusion length and a higher probability of being stabilized by reactions with other species like a Ga adatom before exchanging with a Bi atom. Therefore, this effect is expected to induce a lower probability of Bi exchange and a higher Bi incorporation at lower temperature, consistent with previous experimental findings [24, 25, 27].

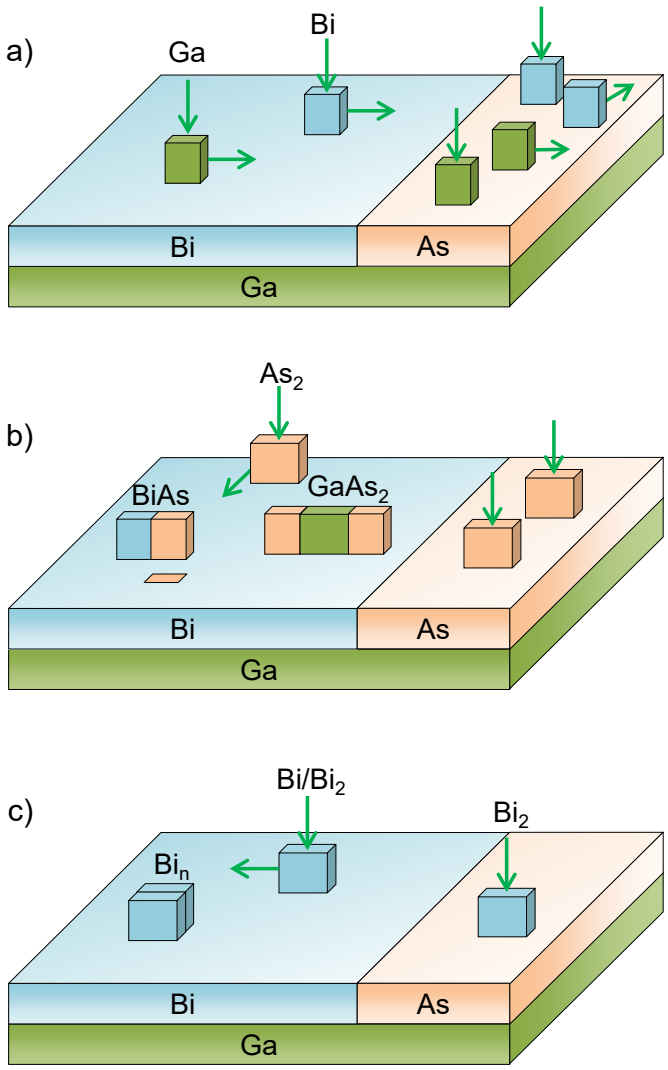

FIG. 7. (Color online) Schematics of processes on the Bi and As surfaces at the initial growth stage of a Ga layer. (a) Deposition and diffusion of Ga and Bi atoms. (b) Deposition and diffusion of As_2, As_2 exchange with the Bi surface, and As_2 reacting with a Ga atom. (c) Deposition and diffusion of Bi/Bi_2 and formation of Bi cluster.

F. Tuning the Exchange Process

Under the typical co-deposition MBE growth mode, the continuous As_2 supply and fast Bi exchange processes lead to frequent Bi exchange and low Bi incorporation. Though low growth temperature can increase Bi incorporation, consistent with analyses described in the previous section, it usually leads to structural, electronic, and optical issues as mentioned in the Introduction. In light of this understanding, here we explore two possible methods to increase the Bi incorporation and maintain a relatively high growth temperature.

The first method we explore for improved $GaAs_{1-x}Bi_x$ growth is reducing the As_2 supply for the exchange process but keeping it available for GaAs formation. This method can be realized by replacing the codeposition MBE mode with the sequential deposition MBE mode, which allows one to turn on/off each beam during growth. To obtain stoichiometric film using the sequential deposition mode requires very stable beam fluxes, which are usually challenging [40]. However, if such stable beam fluxes are obtained, high Bi incorporation could be achieved by periodic sequential deposition of a monolayer of Ga, a sub-monolayer of As, and a sub-monolayer of Bi. Such sequential deposition greatly reduces As_2 for the Bi exchange process and assures Ga atoms to trap the Bi atoms in the film before later exposure to As_2. The optimal amounts of the As and Bi sub-monolayer are unclear *a priori* but can be established by monitoring the Bi incorporation and film quality under different As and Ga amounts. Because the As_2 source for the Bi exchange process is effectively cut off, this method potentially allows one to use a higher growth temperature to reduce the various defects in $GaAs_{1-x}Bi_x$, a serious problem for growth at low temperature.

Besides reducing the As/Bi exchange process, the above-mentioned method may potentially influence the Bi clustering. Assume that one utilizes the sequential deposition method to enhance the Bi incorporation and boosts the growth temperature to reduce the defects. After the deposition of an As sub-monolayer, the surface possibly exhibit the widely found (2×4) or $c(4\times4)\beta$ reconstruction, both of which consist of As dimer rows with As_2 vacancies [51]. Therefore, during the subsequent deposition of a Bi sub-monolayer, Bi_2 may be formed in the As_2 vacancies. However, as long as the As_2 vacancies are well separated, no larger Bi clusters are expected to be formed. Currently, it is unclear if the sequential MBE method would induce more or less Bi clustering than the codeposition MBE method. We encourage further experiments to resolve this subtle issue.

Another method we explore to improve the $GaAs_{1-x}Bi_x$ growth is increasing the barrier of the exchange processes by applying strain to the substrate, which may be realized by gradient Bi doping, direct substrate bending, or attaching to a piezoelectric film [52]. Strain effects have been shown to impact rates of many atomic processes, e.g. catalysis in metallic systems [53-56] and oxygen surface exchange and diffusion [57, 58]. To demonstrate the possible impact of strain, we impose a 4% compressive/tensile strain along the $[0\,\bar{1}\,1]$ and [011] directions with consideration of all four combinations of strains in the two directions and recalculate the As_2 exchange process in Fig. 5a. Energy profiles in Fig. 8a show that the first peak corresponds to the rate-determining barrier and the barrier is influenced quite differently by different strains. The compression along $[0\bar{1}1]$ and tension along [011] increase the barrier to 0.91 eV, which is about 57% higher than the value (0.58 eV) without strain. However, simultaneous tension along both directions has little influence on the barrier, giving a value of about 0.57 eV. This result is somewhat surprising, since intuition and previous thermodynamic study [13]

suggest that the large Bi atoms would be stabilized in GaAs by tension. However, even though the thermodynamic equilibrium solubility is strongly enhanced by biaxial tension [13], the result here indicates that the kinetic barriers do not behave in such a simple manner. The remaining two strain conditions, compression along both directions and tension along [0$\bar{1}$1] combined with compression along [011], have respective barriers of 0.32 and 0.24 eV, which are obviously lower than the two previous strains.

To understand the very different influences of the strains, we first study the dependence of barrier on the energy difference between the initial and final states. As shown in Fig. 8b, the relationship roughly follow the Brønsted-Evans-Polanyi principle [59], which states that the difference in activation barrier between two similar reactions depends linearly on their difference in enthalpy of reaction. In other words, in order to reduce the exchange process kinetically, one needs to reduce the process thermodynamically. In Fig. 8c, we further show the structural changes of the rate-limiting transition state relative to the initial state for the process without strain. It is clear that the major in-plane changes of the transition state are expansion perpendicular to the dimer row and compression parallel to the dimer row. Therefore, it is physically intuitive that one can increase (decrease) the barrier by counteracting (facilitating) the aforementioned structural changes through applying compression (tension) perpendicular to the dimer row and tension (compression) parallel to the dimer row. This strategy is consistent with the findings from the DFT calculations in Fig. 8a.

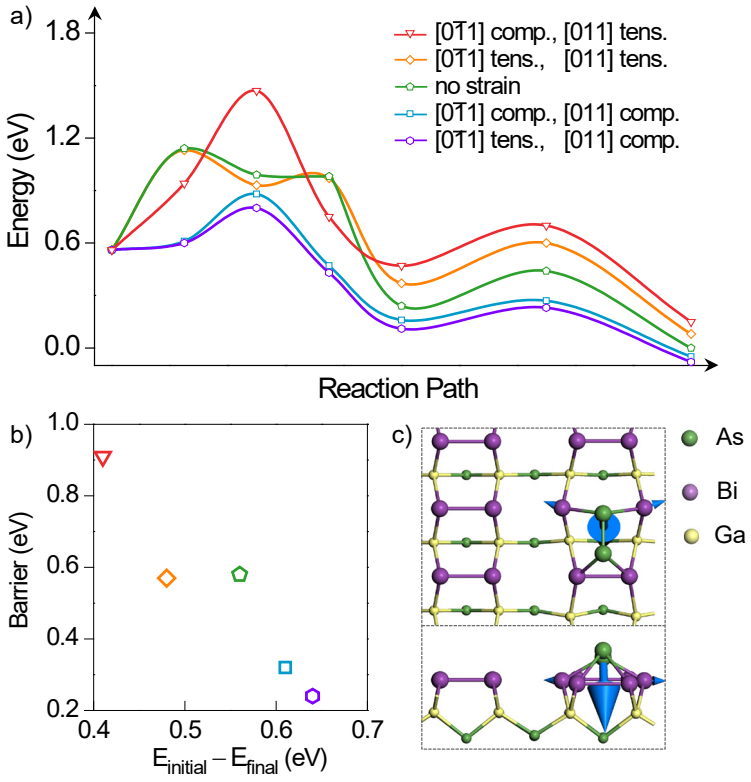

FIG. 8. (Color online) Strain effects on the Bi exchange process. (a) Energy profiles of Bi exchange processes similar to Fig. 5a on substrate with 4% tensile (tens.) or compressive (comp.) strain along $[0\bar{1}1]$ and [011] directions. The case without strain (Fig. 5a) is also shown for comparison. For easy comparison, the profiles are shifted to match their initial states to the no strain case. (b) Energy difference between the initial and final states versus the rate-determining barrier. (c) Atomic displacements of the rate-limiting transition state relative to the initial state for the Bi exchange process without strain. Arrow sizes are proportional to the amplitude of atomic displacements.

IV. SUMMARY AND REMAINING WORK

In summary, we have studied the growth of $GaAs_{1-x}Bi_x$ films under MBE conditions using first-principles calculations. The energetics and kinetics on the (2×1)-Ga_{sub}||Bi surface and a newly proposed q(1×1)-Ga_{sub}||AsAs surface were investigated. All the MBE species were found to display strong chemical adsorption on the two surfaces with low desorption rates. Most ad-species diffuse very quickly on the two surfaces relative to the growth rate, except As_2 and Bi_2 on the As surface. Three essential kinetic processes during the growth, namely, the incorporation, exchange, and clustering of Bi, were explored on the (2×1)-Ga_{sub}||Bi by studying the Ga adsorption, As_2 exchange with the Bi surface, and Bi_2/Bi_3 formation, respectively. All of the three processes show a large driving force and low reaction barriers. The experimental finding of higher Bi incorporation at lower temperature was explained by the higher probability of As_2 reacting with other species before exchange with Bi at a lower temperature. Based on the Bi exchange mechanism, we proposed that an increased Bi incorporation under higher growth temperature may be achieved either by reducing the As_2 supply for the exchange process using the sequential deposition method or by increasing the Bi exchange barrier through applying compressive strain perpendicular to the Bi dimer row and tensile strain parallel to the Bi dimer row.

Finally, we would like to briefly discuss three aspects that are not systematically studied here and may need further investigations. One aspect is that our major calculations are carried out on pure Bi- and As-terminated surfaces, which can be considered as an approximation of the Bi- and As-rich areas of the real surface, respectively. However, at certain growth stages, the surface could be mixed with Bi and As, and the energetic and kinetic processes could exhibit different values from the predictions of this work. Another aspect is that our calculations do not consider the influences of defects, such as As_{Ga}, which are common in $GaAs_{1-x}Bi_x$ films grown at low temperature. When the defects are close to surface, they may impact some processes we have studied, such as ad-species diffusion and As/Bi exchange. Unfortunately, very little is known about the defects in the growing surface. A previous experiment with growth conditions similar to ours found that the dominant defect (a possible complex consisting of As_{Ga} and V_{Ga}) possesses a concentration of ~5×10^{16} cm^{-3} [60], which corresponds to one As_{Ga} defect among ~4×10^5 Ga

sites. Due to this relatively low atomic ratio, defects are unlikely to play a dominant role in the surface growth, although the surface defect concentration will likely be different from that in the bulk. The third aspect is that we have primarily focused on the dynamic processes on the Bi surface and have not investigated the processes on the As surface in detail. This is because the Bi surface is a Bi reservoir and should be the major surface that determines the Bi incorporation. However, the evolution of the As surface is an important topic for future study.

ACKNOWLEDGEMENTS

This research was primarily supported by the NSF-funded University of Wisconsin Materials Research Science and Engineering Center (DMR-1121288). The authors gratefully acknowledge the use of clusters supported by UW MRSEC (DMR-1121288). A portion of theoretical calculations were carried out at the National Energy Research Scientific Computing Center (NERSC), a DOE Office of Science User Facility supported by the Office of Science of the U.S. Department of Energy under Contract No. DE-AC02-05CH11231. Computing resources in this work also benefitted from the use of the Extreme Science and Engineering Discovery Environment (XSEDE), which is supported by National Science Foundation grant number OCI-1053575.

References

[1] A. Belabbes, A. Zaoui, and M. Ferhat, J. Phys. Condens. Matter **20**, 415221 (2008).
[2] D. Madouri, A. Boukra, A. Zaoui, and M. Ferhat, Comp. Mater. Sci. **43**, 818 (2008).
[3] I. Moussa, H. Fitouri, Z. Chine, A. Rebey, and B. El Jani, Semicond. Sci. Tech. **23**, 125034 (2008).
[4] G. Pettinari, A. Polimeni, M. Capizzi, J. H. Blokland, P. C. M. Christianen, J. C. Maan, E. C. Young, and T. Tiedje, Appl. Phys. Lett. **92**, 262105 (2008).
[5] Z. Chine, H. Fitouri, I. Zaied, A. Rebey, and B. El Jani, Semicond. Sci. Technol. **25**, 065009 (2010).
[6] K. Oe, and H. Okamoto, Jpn. J. Appl. Phys. **37**, L1283 (1998).
[7] K. Oe, J. Cryst. Growth **237**, 1481 (2002).
[8] K. Oe, Jpn. J. Appl. Phys. **41**, 2801 (2002).
[9] Y. Takehara, M. Yoshimoto, W. Huang, J. Saraie, K. Oe, A. Chayahara, and Y. Horino, Jpn. J. Appl. Phys. **45**, 67 (2006).
[10] I. Moussa, H. Fitouri, A. Rebey, and B. El Jani, Thin Solid Films **516**, 8372 (2008).
[11] Z. Batool, K. Hild, T. J. C. Hosea, X. Lu, T. Tiedje, and S. J. Sweeney, J. Appl. Phys. **111**, 113108 (2012).
[12] H. Tong, X. Marie, and M. W. Wu, J. Appl. Phys. **112**, 063701 (2012).
[13] H. Jacobsen, B. Puchala, T. F. Kuech, and D. Morgan, Phys. Rev. B **86**, 085207 (2012).
[14] B. Cordero, V. Gomez, A. E. Platero-Prats, M. Reves, J. Echeverria, E. Cremades, F. Barragan, and S. Alvarez, Dalton Trans., 2832 (2008).
[15] H. Fitouri, I. Moussa, A. Rebey, and B. El Jani, Microelectron. Eng. **88**, 476 (2011).
[16] Z. Chine, H. Fitouri, I. Zaied, A. Rebey, and B. El Jani, J. Cryst. Growth **330**, 35 (2011).

[17] H. Fitouri, I. Moussa, A. Rebey, A. Fouzri, and B. El Jani, J. Cryst. Growth **295**, 114 (2006).
[18] H. Fitouri, I. Moussa, A. Rebey, and B. El Jani, J. Cryst. Growth **300**, 347 (2007).
[19] S. Tixier, M. Adamcyk, T. Tiedje, S. Francoeur, A. Mascarenhas, P. Wei, and F. Schiettekatte, Appl. Phys. Lett. **82**, 2245 (2003).
[20] R. France, C. S. Jiang, and A. J. Ptak, Appl. Phys. Lett. **98**, 101908 (2011).
[21] R. France, and A. J. Ptak, J. Vac. Sci. Technol. B **29**, 03C115 (2011).
[22] S. Francoeur, M. J. Seong, A. Mascarenhas, S. Tixier, M. Adamcyk, and T. Tiedje, Appl. Phys. Lett. **82**, 3874 (2003).
[23] R. B. Lewis, D. A. Beaton, X. Lu, and T. Tiedje, J. Cryst. Growth **311**, 1872 (2009).
[24] V. Pacebutas, K. Bertulis, G. Aleksejenko, and A. Krotkus, J. Mater. Sci.-Mater. Electron. **20**, 363 (2009).
[25] X. Lu, D. A. Beaton, R. B. Lewis, T. Tiedje, and M. B. Whitwick, Appl. Phys. Lett. **92**, 192110 (2008).
[26] X. Lu, D. A. Beaton, R. B. Lewis, T. Tiedje, and Y. Zhang, Appl. Phys. Lett. **95**, 041903 (2009).
[27] R. B. Lewis, M. Masnadi-Shirazi, and T. Tiedje, Appl. Phys. Lett. **101**, 082112 (2012).
[28] G. Vardar, S. W. Paleg, M. V. Warren, M. Kang, S. Jeon, and R. S. Goldman, Appl. Phys. Lett. **102**, 042106 (2013).
[29] V. Pačebutas, R. Butkutė, B. Čechavičius, J. Kavaliauskas, and A. Krotkus, Thin Solid Films **520**, 6415 (2012).
[30] J. C. Li, T. H. Kim, K. Forghani, W. Y. Jiao, W. Kong, K. Collar, T. F. Kuech, and A. S. Brown, J. Appl. Phys. **116**, 043524 (2014).
[31] M. Masnadi-shirazi, D. A. Beaton, R. B. Lewis, X. Lu, and T. Tiedje, J. Cryst. Growth **338**, 80 (2012).
[32] M. Ahola-Tuomi, P. Laukkanen, R. E. Perälä, M. Kuzmin, J. Pakarinen, I. J. Väyrynen, and M. Adell, Surf. Sci. **600**, 2349 (2006).
[33] G. Kresse, and J. Furthmuller, Phys. Rev. B **54**, 11169 (1996).
[34] G. Kresse, and D. Joubert, Phys. Rev. B **59**, 1758 (1999).
[35] See Supplemental Materials for influence of spin-orbit coupling to binding energy and activation barrier, exchange of Ga adatom with Bi of (2×1)-Ga_{sub}||AsBi surface, minimal energy potential of desorption, exchange of As_2 with Bi in (2×1)-Ga_{sub}||As surface, exchange of Ga adatom with Bi of (2×1)-Ga_{sub}||Bi surface, and animations of selected dynamic processes.
[36] X. Huang, E. Lindgren, and J. Chelikowsky, Phys. Rev. B **71**, 165328 (2005).
[37] K. Shiraishi, J. Phys. Soc. Jpn. **59**, 3455 (1990).
[38] G. Henkelman, B. P. Uberuaga, and H. Jonsson, J. Chem. Phys. **113**, 9901 (2000).
[39] F. Bastiman, A. G. Cullis, J. P. R. David, and S. J. Sweeney, J. Cryst. Growth **341**, 19 (2012).
[40] M. Henini, *Molecular Beam Epitaxy: From Research to Mass Production* (Elsevier Science, 2012).
[41] P. Laukkanen, M. Punkkinen, H.-P. Komsa, M. Ahola-Tuomi, K. Kokko, M. Kuzmin, J. Adell, J. Sadowski, R. Perälä, M. Ropo, T. Rantala, I. Väyrynen, M. Pessa, L. Vitos, J. Kollár, S. Mirbt, and B. Johansson, Phys. Rev. Lett. **100**, 086101 (2008).

[42] M. Punkkinen, P. Laukkanen, H.-P. Komsa, M. Ahola-Tuomi, N. Räsänen, K. Kokko, M. Kuzmin, J. Adell, J. Sadowski, R. Perälä, M. Ropo, T. Rantala, I. Väyrynen, M. Pessa, L. Vitos, J. Kollár, S. Mirbt, and B. Johansson, Phys. Rev. B **78**, 195304 (2008).
[43] A. Duzik, J. C. Thomas, A. van der Ven, and J. M. Millunchick, Phys. Rev. B **87**, 035313 (2013).
[44] S. Hirose, S. Haneda, M. Yamaura, K. Hara, and H. Munekata, J. Vac. Sci. Technol. B **18**, 1397 (2000).
[45] O. Romanyuk, P. Jiricek, M. Cukr, and I. Bartos, Czech. J. Phys. **53**, 49 (2003).
[46] C. G. Morgan, P. Kratzer, and M. Scheffler, Phys. Rev. Lett. **82**, 4886 (1999).
[47] K. K. Wang, and A. R. Smith, Comput. Phys. Commun. **182**, 2208 (2011).
[48] M. Dell'Angela, T. Anniyev, M. Beye, R. Coffee, A. Fohlisch, J. Gladh, T. Katayama, S. Kaya, O. Krupin, J. LaRue, A. Mogelhoj, D. Nordlund, J. K. Norskov, H. Oberg, H. Ogasawara, H. Ostrom, L. G. M. Pettersson, W. F. Schlotter, J. A. Sellberg, F. Sorgenfrei, J. J. Turner, M. Wolf, W. Wurth, and A. Nilsson, Science **339**, 1302 (2013).
[49] Y. N. Mo, W. G. Zhu, E. Kaxiras, and Z. Y. Zhang, Phys. Rev. Lett. **101**, 216101 (2008).
[50] R. D. Richards, F. Bastiman, C. J. Hunter, D. F. Mendes, A. R. Mohmad, J. S. Roberts, and J. P. R. David, J. Cryst. Growth **390**, 120 (2014).
[51] A. Ohtake, Surf. Sci. Rep. **63**, 295 (2008).
[52] G. X. Bai, Y. Zhang, and J. H. Hao, Sci. Rep. **4**, 5724 (2014).
[53] J. Greeley, and M. Mavrikakis, Nat. Mater. **3**, 810 (2004).
[54] M. Mavrikakis, B. Hammer, and J. K. Norskov, Phys. Rev. Lett. **81**, 2819 (1998).
[55] L. Grabow, Y. Xu, and M. Mavrikakis, Phys. Chem. Chem. Phys. **8**, 3369 (2006).
[56] Y. Xu, and M. Mavrikakis, J. Phys. Chem. B **107**, 9298 (2003).
[57] M. Kubicek, Z. H. Cai, W. Ma, B. Yildiz, H. Hutter, and J. Fleig, ACS Nano **7**, 3276 (2013).
[58] T. Mayeshiba, and D. Morgan, Phys. Chem. Chem. Phys. **17**, 2715 (2015).
[59] V. Brázdová, and D. R. Bowler, *Atomistic computer simulations: a practical guide* (Wiley-VCH, Weinheim, 2013), p. 361.
[60] P. M. Mooney, K. P. Watkins, Z. Jiang, A. F. Basile, R. B. Lewis, V. Bahrami-Yekta, M. Masnadi-Shirazi, D. A. Beaton, and T. Tiedje, J. Appl. Phys. **113**, 133708 (2013).